7820–7830 *Nucleic Acids Research, 2018, Vol. 46, No. 15* *Published online 13 July 2018*
doi: 10.1093/nar/gky619

The ribosomal stalk protein is crucial for the action of the conserved ATPase ABCE1

Hirotatsu Imai, Takaya Abe, Tomohiro Miyoshi, Shuh-ichi Nishikawa, Kosuke Ito and Toshio Uchiumi*

Department of Biology, Faculty of Science, Niigata University, Ikarashi 2–8050, Nishi-ku, Niigata 950–2181, Japan

Received March 19, 2018; Revised June 25, 2018; Editorial Decision June 26, 2018; Accepted June 28, 2018

ABSTRACT

The ATP-binding cassette (ABC) protein ABCE1 is an essential factor in ribosome recycling during translation. However, the detailed mechanochemistry of its recruitment to the ribosome, ATPase activation and subunit dissociation remain to be elucidated. Here, we show that the ribosomal stalk protein, which is known to participate in the actions of translational GTPase factors, plays an important role in these events. Biochemical and crystal structural data indicate that the conserved hydrophobic amino acid residues at the C-terminus of the archaeal stalk protein aP1 binds to the nucleotide-binding domain 1 (NBD1) of aABCE1, and that this binding is crucial for ATPase activation of aABCE1 on the ribosome. The functional role of the stalk•ABCE1 interaction in ATPase activation and the subunit dissociation is also investigated using mutagenesis in a yeast system. The data demonstrate that the ribosomal stalk protein likely participates in efficient actions of both archaeal and eukaryotic ABCE1 in ribosome recycling. The results also show that the stalk protein has a role in the function of ATPase as well as GTPase factors in translation.

INTRODUCTION

The process of translation on the ribosome is composed of four successive steps, initiation, elongation, termination and recycling. It is well established that in the three domains of life, initiation, elongation and termination steps are promoted by actions of individual translational GTPase factors (1–3), and that a specific ribosomal component termed the stalk protein stimulates recruitment of most of these GTPases to a common ribosomal site, the factor-binding center and activates the coupled GTP hydrolysis (3–5). The recycling step has diverged during evolution, i.e. the bacterial ribosomal recycling requires ribosome recycling factor together with a GTPase, EF-G, whereas the eukaryotic and archaeal recycling step requires the ABC-type adenosine triphosphatase (ATPase) ABCE1 (6). Through the action of eukaryotic/archaeal ABCE1, ribosomes dissociate into large and small subunits in an ATP-dependent manner either after the termination step via release factors or after binding of the termination factor paralog Pelota to stalled ribosomes (7–10). Interestingly, ABCE1-dependent ribosome splitting occurs in other cellular pathways. In nutrition stress, vacant ribosomes accumulate to prevent protein biosynthesis, and they are split by ABCE1 after stress release (10,11). Furthermore, in eukaryotic ribosome biogenesis, 80S-like ribosomal complex are formed and subsequent split by ABCE1 as a means of quality control (12). However, the detailed molecular mechanism of these action of ABCE1 is still obscure.

ABCE1 contains two nucleotide-binding domains (NBD1/NBD2) oriented in a head-to-tail fashion and linked by hinge 1 and 2 regions. Also, it's unique N-terminal iron-sulfur cluster domain (FeS) contains two $[4Fe\text{-}4S]^{2+}$ clusters (13,14). It is anticipated that NBD1 and NBD2 undergoes a tweezers-like motion cycling between the ATP-bound closing state and ADP-bound opening state, that is typical of ABC proteins. ATP hydrolysis seems to provide the 'power stoke' through the conformational change involved in ribosome disassembly into subunits. Cryo-EM study of archaeal 70S•aPelota•aABCE1 complexes in the pre-splitting state revealed that ABCE1 directly binds to ribosomes in the inter-subunit space covering the factor-binding center, where translational GTPases, such as EF1A and EF2, bind, and that ABCE1 adopts an intermediate, half-open state of the two NBDs (15–17). More recent cryo-EM analysis showed that in the post-splitting state ABCE1 binds to the small subunit and adopts the closed state of the two NBDs with AMP-PNP (18). These studies also suggested that movement of the FeS domain of ABCE1 is involved in subunit dissociation in ribosome recycling (6,9,16–19).

With respect to the mechanism of function of ABCE1 in ribosome recycling, intriguing questions remain. These include how ABCE1 is recruited to the ribosome and what triggers its ATP hydrolysis. Many lines of evidence have

*To whom correspondence should be addressed. Tel: +81 25 262 7792; Fax: +81 25 262 7792; Email: uchiumi@bio.sc.niigata-u.ac.jp

suggested that multiple copies of the ribosomal stalk protein play a crucial role in efficient recruitment of GTPase translation factors to the ribosomal factor binding center and activation of GTP hydrolysis (3–5), whereas there is no experimental evidence for the functional role of the stalk protein in ABCE1 action. We have established assay systems to study the structure and function of the eukaryotic and archaeal ribosomal stalk proteins and have reported the following findings: (i) the stalk exist in an oligomeric form, namely as a $aP0(aP1)_2(aP1)_2(aP1)_2$ heptamer in archaea (20,21) or P0(P1-P2)(P1-P2) pentamer in eukaryotes (22); (ii) the C-terminal half of each stalk protein is flexible and moves around the ribosome (23); (iii) the conserved C-terminal end region of the aP1 directly binds to GTPase translation factors (24,25); (iv) each stalk protein participates in recruitment of GTPase factors to the sarcin/ricin loop of 23S/28S rRNA within the factor binding center and in activation of GTP hydrolysis (26,27).

In the present study, we show that the C-terminal region of the aP1 stalk protein binds to the NBD1 of aABCE1 and activates its ribosome-dependent ATP hydrolysis in the presence of aPelota. The mode of binding of the aP1 to NBD1 of aABCE1 was clarified by crystal structural analysis, and the structural data pertaining to the aP1•aABCE1 binding is confirmed by functional assays using various mutants. Furthermore, the functionality of this interaction is also confirmed by using yeast system. Our results suggest that the ribosomal stalk protein participates in recruitment of archaeal and eukaryotic ABCE1 and subsequent ATPase activation that leads to ribosome splitting.

MATERIALS AND METHODS

Plasmid constructions and protein purification

The plasmids for expression of *Pyrococcus horikoshii* aL11, aP0, aP1 and their mutants were constructed, and the proteins were expressed and purified as described previously (21,28). The plasmid for expression of N-terminal maltose binding protein (MBP) fused with the C-terminal half of aP1, MBP-aP1[61–108], was constructed by insertion of the coding sequence for residues 61–108 of aP1, (amplified from the *Pyrococcus furiosus* (DSM3638) genome by polymerase chain reaction (PCR)) between the EcoRI and HindIII sites in the pMAL-c4x vector. The resultant plasmid pMAL-c4x-aP1[61–108] was used as a template for PCR to construct the truncation mutant MBP-aP1[61–90] lacking the sequence for residues 91–108 of aP1. Recombinant MBP-aP1[61–108] and MBP-aP1[61–90] proteins were expressed in *Escherichia coli* BL21 (DE3) codon plus RIL by adding 0.5 mM IPTG. After incubation at 37°C for 3 h, cells were harvested by centrifugation, resuspended in Lysis buffer (20 mM HEPES-KOH pH7.6, 1 M NH_4Cl, 5% (v/v) glycerol, 7 mM 2-ME) and disrupted by sonication. After sedimenting cell debris and other insoluble materials, MBP-aP1[61–108] and MBP-aP1[61–90] were purified by amylose-affinity chromatography and size-extraction chromatography. The coding sequences of aABCE1 and aPelota were amplified by PCR from the *P. furiosus* (DSM3638) genome and inserted between NdeI and BamHI sites of pET28b and pET15a, respectively. Plasmids for aABCE1-mutants were generated by PCR site-directed mutagenesis using pET28b-aABCE1 as a template. The protein expression and disruption of *E. coli* cells were as described above for the fusion proteins, except that IPTG-induction of protein expression was performed at 18°C for 20 h. The expressed proteins were purified by heat treatment (70°C for 20 min) of cell extracts, Ni-affinity chromatography, anion-exchange and size-extraction chromatography.

The plasmid for expression of Rli1 (pYES2-Rli1) was kindly provided by Rachel Green (Department of Molecular Biology and Genetics, Johns Hopkins University School of Medicine). The plasmid for expression of Rli1-3S mutant was generated *by* PCR site-directed mutagenesis. Rli1 (WT and 3S mutant) proteins were expressed in *Saccharomyces cerevisiae* and purified as described previously (8). The plasmid for expression of Dom34 was constructed by replacing the coding sequence of yEGFP in the pTOW-p-GFP plasmid, which was kindly provided by Hisao Moriya (Research Core for Interdisciplinary Sciences, Okayama University), with the coding sequence of Dom34-His (amplified from the *S. cerevisiae* (W303-1A) genome by PCR). The protein was expressed in *S. cerevisiae* INVSc1 strain at 30°C for 16 h in SCD-Ura-Leu medium. After cell disruption, Dom34 was purified by Ni-affinity chromatography and size-extraction chromatography. The plasmid for expression of eukaryotic initiation factor 6 (eIF6) was constructed by insertion of the coding sequence (amplified from the *S. cerevisiae* (W303-1A) genome by PCR) between the NdeI and BamHI sites in the pET28b vector. Recombinant eIF6 protein was induced in *E. coli* BL21 (DE3) codon plus RIL by adding 0.5 mM IPTG. After incubation at 18°C for 20 h, cells were harvested and the protein was purified by Ni-affinity chromatography.

Native-PAGE

Pyrococcus horikoshii ribosomal protein aP1 was radiolabeled by phosphorylation using [γ-^{32}P] ATP and casein kinase II (New England Biolabs) at 30°C for 30 min (22). [^{32}P]-labeled aP1 was mixed with increasing amounts of aABCE1 and was subjected to gel electrophoresis as described previously (24).

ATPase measurement using hybrid ribosomes

The hybrid ribosome containing aL11, aP0 and aP1 were formed as described previously (Nomura *et al.*, (28)). 100 pmol of aABCE1, aPelota and 10 pmol of the hybrid 70S ribosome were incubated with 1000 pmol of [γ-^{32}P] ATP in 100 μl of ATPase buffer (20 mM Tris–HCl pH 7.6, 50 mM NH_4Cl, 10 mM $MgCl_2$, 1 mM DTT) at 37°C for 20 min. The inorganic phosphate liberated was assayed as described previously (29).

Pull-down assay

aABCE1 (1000 pmol) was mixed with equal amounts of MBP-aP1[61–108] or MBP-aP1[61–90] in 100 μl of PD buffer (20 mM Tris–HCl pH 7.6, 200 mM NaCl, 7 mM 2-ME). Subsequently, 20 μl of amylose resin (New England Biolabs) was added to the mixture. After incubation with a rotation speed of 5 rpm at 4°C for 90 min, the beads were

washed twice with 500 μl of PD buffer and then bound proteins were co-eluted with 40 μl of PD buffer containing 50 mM maltose. The eluted proteins were analyzed by sodium dodecyl sulphate-polyacrylamide gel electrophoresis (SDS-PAGE), followed by CBB staining.

Fluorescence polarization binding assay

The peptide comprising the C-terminal 18 amino acid residues EEEVSEEEALAGLSALFG of aP1, whose N-terminus was labeled with fluorescein isothiocyanate (FITC), was purchased from Hokkaido System Science Co., Ltd. (Hokkaido, Japan). The FITC-labeled peptide (5 nmol) was mixed with 0, 2.5, 5, 10, 20, 40, 80, 160 μM of aABCE1 in 100 μl of FP buffer (20 mM HEPES-KOH pH 7.6, 10 mM $MgCl_2$, 200 mM KCl, 7 mM 2-ME, 0.1 mg/ml bovine serum albumin). All measurements were performed at 25°C using a Pan Vera Beacon 2000 fluorescence polarization instrument (Invitrogen). Curve fitting was carried out by nonlinear regression using saturation binding—one site specific binding in GraphPad Prism 6 for MacOS, GraphPad Software, San Diego California USA.

Crystallization, data collection and structure determination

Crystals of the aABCE1-ΔN74•ADP•aP-C18 complex was prepared by the sitting drop vapor diffusion method at 20°C by mixing 1 μl of protein solution (10 mg/ml aABCE1-ΔN74, 2 mg/ml aP-C18 peptide, 1 mM ADP, 10 mM Tris–HCl pH 8.0, 10 mM $MgCl_2$, 150 mM NaCl) and equal volume of reservoir solution [100 mM HEPES pH 7.0, 15% (w/v) PEG4000, 10% (v/v) 2-propanol]. Diffraction data were collected with a wavelength of 1.54 Å at 100 K using a Rigaku RAXIS IV^{++} image plate detector mounted on a Rigaku Micromax-007HF generator and processed with XDS (30). The initial model of the aABCE1-ΔN74•ADP•aP-C18 complex was obtained by the molecular replacement method using BALBES (31). The model was then manually refined using COOT and REFMAC5 (32,33). The resultant data collection and refinement statistics are summarized in Supplementary Table S1. Structural figures were prepared using CueMol2 (http://www.cuemol.org/en/).

Yeast 80S ribosomes, their Rli1-dependent ATPase activity and subunit dissociation

Yeast 80S ribosomes were prepared as described previously (34). ATP hydrolysis was performed as follows. A total of 10 pmol of Rli1, Dom34 and 1 pmol of 80S ribosome were incubated with 1000 pmol of [γ-^{32}P] ATP in 20 μl of ATPase buffer (20 mM Tris–HCl pH 7.6, 5 mM MgOAc, 100 mM KOAc, 0.5 mM spermine, 1 mM DTT) at 30°C for 10 min. The inorganic phosphate liberated was assayed as described previously (29). Subunit dissociation was performed as follows. A total of 10 pmol of 80S ribosome were incubated with 50 pmol of eIF6, Dom34 and Rli1 (WT or 3S mutant) in 50 μl of SP buffer (20 mM Tris–HCl pH 7.6, 2.5 mM MgOAc, 100 mM KOAc, 0.5 mM spermine, 1 mM DTT, 1 mM ATP or AMP-PNP) at 30°C for 5 min. Samples were loaded in SP buffer containing 15–30% sucrose density gradient and centrifuged in a S100AT4-580 rotor (Hitachi Co. Ltd.) at 163 000 g and 4°C for 150 min. The ribosome UV (254 nm) profile was recorded using a BIO-MINI UV MONITOR AC-5200 (ATTO). Subunits/Monosome ratios were determined as described previously (35).

Co-sedimentation assay

The hybrid ribosomes (50 pmol) were incubated with equal amounts of aABCE1 and aPelota in 50 μl of PL buffer (56 mM Tris–HCl pH 8.0, 250 mM KCl, 80 mM NH_4Cl, 50 mM $MgCl_2$, 1 mM DTT, 0.5 mM spermin, 2 mM AMP-PNP) at 37°C for 10 min. Samples were loaded in 950 μl of PL buffer containing 34.2% sucrose and centrifuged with a S100AT4-580 rotor (Hitachi Co. Ltd.) at 189 000 g and 4°C for 30 min. Samples of ribosomal pellets (P) and supernatant fractions collected by TCA precipitation (S) were analyzed by SDS-PAGE, followed by CBB staining.

DMS footprinting assay

The hybrid ribosomes (20 pmol) were incubated with 200 pmol each of aABCE1 and aPelota in 50 μl of CM buffer (100 mM potassium cacodylate pH 7.2, 50 mM NH_4Cl, 10 mM $MgCl_2$, 1 mM DTT, 0.5 mM spermin, 2 mM AMP-PNP) at 37°C for 10 min. Subsequently, 2 μl of dimethyl sulfate (1:4 dilution in ethanol) was added to each ribosome sample and incubated at 37°C for 10 min. The modified rRNA was collected by phenol–chloroform extraction and ethanol precipitation, and then analyzed by primer extension followed by gel electrophoresis as described previously (36).

Yeast plasmids and strains construction

Yeast plasmids and strains used in this study are listed in Supplementary Tables S3 and 4, respectively. pTU1002 was constructed as follows. A DNA fragment for the GAL1 promoter (P_{GAL1}) was amplified from pYES2 vector. DNA fragments for ubiquitin with an arginine residue added to the C-terminus (*UBI-R*), and Rli1 with N-terminal FLAG-tag (*FLAG-RLI1*) were amplified from *S. cerevisiae* W303-1A genome. The P_{GAL1}-*UBI-R-FLAG-RLI1* fragment was obtained by PCR reactions using the DNA fragments of P_{GAL1}, *UBI-R* and *FLAG-RLI1* as templates and primers, and introduced into the *Bam*HI site of YCplac111 using Seamless Ligation Cloning Extract (SLiCE) from *E. coli*, as described previously (37). pTU1004 was constructed as follows. The DNA fragment of P_{GAL1}-*UBI-R* was amplified from pTU1002 and introduced into pFA6-kanMX using the SLiCE reaction. A DNA fragment of *RLI1* containing + 662 bp of 5′UTR and + 400 bp of 3′UTR was amplified from *S. cerevisiae* W303-1A genome and introduced into the BamHI site of YCplac22 using SLiCE as described above to construct pTU2001. pTU2002 was constructed by inserting a DNA fragment of 3HA, which was amplified from pFA6a-kanMX-P_{GAL1}-3HA, into pTU2001. pTU2003 was generated by site-directed mutagenesis using pTU2002 as template. The YTU2001 (*rli1-deg*) strain

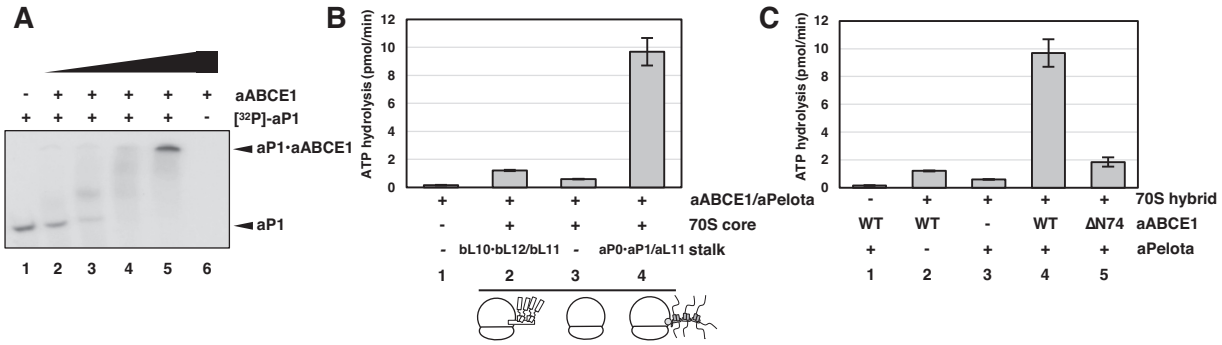

Figure 1. Interaction of archaeal ribosomal stalk protein with aABCE1 and its effect on ribosome-dependent ATPase hydrolysis. (**A**) [^{32}P]-labeled aP1 was incubated with 10, 20, 40 and 80 μg of aABCE1 (lanes 2, 3, 4 and 5, respectively) or without aABCE1 (lane 1). Lane 6, 80 μg of aABCE1 alone. All samples were subjected to Native-PAGE, followed by autoradiography. (**B**) aABCE1 and aPelota were incubated without any ribosome sample (bar 1) or with *Escherichia coli* 70S core supplemented with *E. coli* bL10•bL12/bL11 proteins (bar 2), no protein (bar 3) and *Pyrococcus furiosus* aP0•aP1/aL11 proteins (bar 4). The samples were then assayed for ATP hydrolysis activity, as described in 'Materials and Methods' section. (**C**) Effect of presence of aPelota and deletion of the N-terminal FeS-domain of aABCE1 (residues 1–74) on ATP hydrolysis. The hybrid ribosomes carrying *P. furiosus* aP0•aP1/aL11 proteins were incubated with aABCE1-WT alone (bar 2), aPelota alone (bar 3), aABCE1-WT and aPelota (bar 4) and aABCE1-ΔN74 and aPelota (bar 5). Subsequently, ATP hydrolysis activity was assayed, as in (B). The averages and standard deviations of five independent assays are shown in (B) and (C). Bar 1 and bar 4 in (B) and (C) show the same respective data.

was constructed as follows. The DNA fragment of *KanMX-P$_{GAL1}$-UBI-R-FLAG* was amplified from pTU1004 by PCR and transformed into yeast W303-1A strain.

Western blotting

Yeast cells were cultured overnight to OD_{600} of 1.0 ∼ 1.5 (log phase), harvested by centrifugation, washed and resuspended in fresh YPD (2% glucose) medium to an OD_{600} of 0.01 for *rli1*-deg strains. Cells were grown in YPD for 16 h to deplete UBI-R-FLAG-Rli1, harvested by centrifugation and frozen in liquid N_2. Cell extracts were analyzed by SDS-PAGE and western blotting using the indicated antibodies. An anti-Tom40 antibody was kindly provided from Toshiya Endo (Faculty of Life Sciences, Kyoto Sangyo University).

RESULTS

Functional interaction of the aP1 stalk protein with aABCE1

The isolated archaeal ribosomal stalk protein aP1 and aABCE1 were mixed and their binding was examined by native gel electrophoresis. To monitor the mobility shift of aP1 upon aABCE1 binding, aP1 was labeled with ^{32}P at Ser95 (22,38). By adding increasing amounts of aABCE1, the band of free aP1 (Figure 1A, lane 1) was shifted toward the top of the gel (lanes 2–5), suggesting an interaction of aP1 with aABCE1. To investigate the functional significance of this aP1•aABCE1 binding, we used hybrid ribosomes, in which the bL12 stalk protein, bL10 and bL11 of the *E. coli* 50S subunit were replaced *in vitro* with their archaeal counterparts (designated here as aP1, aP0 and aL11, respectively). In previous studies, we successfully used these hybrid ribosomes to demonstrate the functional roles of archaeal and eukaryotic stalk proteins, as follows: (i) in recruitment of their cognate elongation factors to the SRL of 23S/28S rRNA (26,27); (ii) in activation of the factor-dependent GTP hydrolysis (24–27,39); (iii) in translation elongation dependent on elongation factors (26,39). Because the hybrid ribosomes have proved useful and produced solid data on the functional roles of archaeal and eukaryotic stalk proteins, we here used the hybrid system to test the role of aP1 in ribosome-dependent ATPase activity of aABCE1 in the presence of aPelota. As shown in Figure 1B, only low levels of ATPase activity were detected with archaeal aABCE1•aPelota alone (bar 1) or with aABCE1•aPelota with *E. coli* ribosome (70S core + bL12 + bL10 + bL11, bar 2) and with the *E. coli* core ribosome lacking bL12, bL10 and bL11 (bar 3). However, the ATPase activity was markedly enhanced by addition of the aP0•aP1 stalk protein complex and aL11 to *E. coli* core to make the hybrid ribosome (bar 4). Furthermore, the ATPase activity was observed in a time and aABCE1-dose-dependent manner (Supplementary Figure S1A and B). The results in Figure 1A and B suggest that aP1 interacts with aABCE1 and participates in its ribosome-dependent ATPase function. To evaluate whether the aP1-dependent ATPase activation of the hybrid ribosome reflects an actual functional characteristic of aABCE1, we investigated the effects of deletion of the N-terminal FeS domain of aABCE1, the interaction of which with aPelota is crucial for ribosome binding (6,9,15–18). The results demonstrate that aP1-dependent ATPase activation of the hybrid ribosome completely depends on the N-terminal FeS domain in aABCE1 and the presence of aPelota (Figure 1C). These observations are consistent with previous biochemical studies using intact ribosomes (8,9). Therefore, it is likely that the aP1-dependent ATPase activation of aABCE1 observed with the hybrid ribosome reflects a true functional characteristic of aABCE1.

Role of the C-terminal region of the stalk protein in aABCE1 recruitment

Recent studies have shown that the conserved C-terminal region of the archaeal/eukaryotic stalk protein is responsible for recruitment of translational GTPase factors to the ribosome and the associated GTP hydrolysis (24–27). To examine the role of the C-terminal region of the aP1 in the binding to aABCE1, we constructed fusion proteins

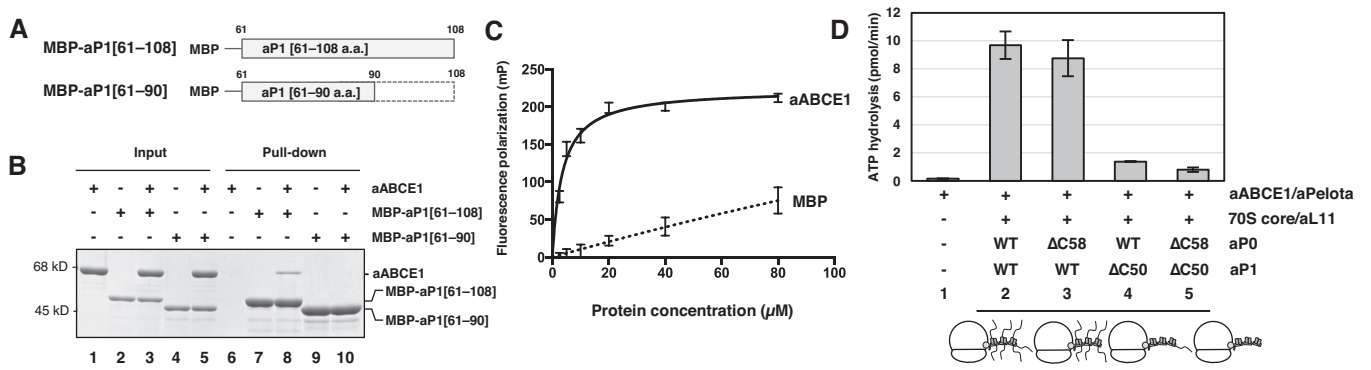

Figure 2. Roles of the C-terminus of aP1 in aABCE1 binding and ATPase activation. (**A**) Schematic representation of two fusion proteins composed of MBP fused with the C-terminal amino acids residues 61–108 (MBP-aP1[61–108]) and residues 61–90 (MBP-aP1[61–90]) of aP1. (**B**) *In vitro* pull-down assay using amylose resin. Protein samples indicated at the top of the gel were mixed without (lanes 1–5) or with amylose resin (lanes 6–10). A portion of input samples (lanes 1–5) and protein samples bound to amylose resin (lanes 6–10) were subjected to SDS-PAGE. The proteins were detected by CBB staining. (**C**) Fluorescence polarization assay for binding of the FITC-labeled aP-C18 peptide to aABCE1. The labeled peptide was mixed with various concentrations of aABCE1 (or MBP as a negative control), and mP values were determined for each protein concentration. The averages and standard deviations of three independent experiments are shown. (**D**) ATP hydrolysis activity of aABCE1 with hybrid ribosomes carrying aP0/aP1 mutants. The hybrid ribosomes were formed by incubation of *Escherichia coli* 70S core with aL11, together with WT aP0 and WT aP1 (bar 2), with aP0 lacking the C-terminal 58 amino acid residues (aP0-ΔC58) and WT aP1 (bar 3), with WT aP0 and aP1 lacking the C-terminal 50 amino acid residues (aP1-ΔC50) (bar 4) and with aP0-ΔC58 and aP1-ΔC50 (bar 5). These samples were assayed for ATP hydrolysis activity by addition of aABCE1, together with aPelota. The averages and standard deviations of three independent experiments are shown. Bar 1 and bar 2 of Figure 2D show the same data presented by bar 1 and bar 4 of Figure 1B, respectively.

Table 1. Effect of mutations in aABCE1 on aP1 binding

aABCE1	K_d for aP-C18 (μM)[a]	K_d ratio[b]
WT	3.9 ± 0.3	1
ΔN74	4.4 ± 0.2	1.1
I170S	68.1 ± 8.2	17.5
V174S	83.0 ± 5.0	21.3
V219S	6.3 ± 0.2	1.6
A223S	46.3 ± 1.3	11.9
R227A	30.8 ± 3.2	7.9

[a]Errors are SD of values calculated from three independent experimental replicates.
[b]K_d ratio = $K_{d\,(mutant)}/K_{d\,(WT)}$ for FITC-labeled aP-C18.

containing MBP fused with the C-terminal half of aP1 (MBP-aP1[61–108]) and the same fusion protein lacking the C-terminal 18 residues (MBP-aP1[61–90]) (Figure 2A), and used these in a pull-down assay with amylose resin. As shown in Figure 2B, aABCE1 was co-precipitated with the MBP-aP1[61–108] fusion protein (lane 8), but not with MBP-aP1[61–90] (lane 10), implying that the C-terminal 18 amino acids region of aP1 includes the binding site of aABCE1. To confirm whether the C-terminal 18 amino acid fragment of aP1 (aP-C18) retains binding ability for aABCE1, we also tested binding between aABCE1 and a fluorescently labeled aP-C18 peptide by fluorescence polarization assay. The result showed a typical binding curve for aABCE1, but not for MBP used as a negative control (Figure 2C). Assuming that aABCE1 has one binding site for aP1, the K_d value is calculated as 3.9 μM (Table 1; details are described below).

The functional significance of the binding of aABCE1 to the C-terminus of aP1 was examined using the hybrid ribosome system. We first confirmed binding of aABCE1 to the hybrid ribosome in the presence of aPelota, but not to the hybrid ribosome carrying an aP1 variant lacking the C-terminal domain (ΔCTD) using a pelleting assay (Supplementary Figure S2A, lanes 14 and 16). To confirm whether aABCE1 together with aPelota binds not only to the stalk protein within the hybrid ribosome, but also to rRNA of the ribosomal core body, we performed DMS-footprint analysis. In this assay, aABCE1 together with aPelota protected base A334 (*E. coli* numbering) in helix 14 of 16S rRNA (Supplementary Figure S2B, lane 7), which is one of the binding sites of aABCE1 observed in the previous cryo-EM study (15). However, this protection of A334 was not observed in the hybrid ribosome carrying the aP1ΔCTD variant. These results suggest that the C-terminal region of aP1 is responsible for recruitment of aABCE1 to the ribosomal body, presumably at or near the factor binding center.

We next investigated the functional role of the C-terminal region of aP1 in the activation of aABCE1 ATPase on the hybrid ribosome (Figure 2D and Supplementary Figure S1). High ATP hydrolysis activity of aABCE1 dependent on WT archaeal aP0•aP1 stalk complex (Figure 2D, bar 2) was markedly reduced by deletion of the C-terminal domain of all copies of aP1 (Figure 2D, bar 4; Supplementary Figure S1), but only slight reduction was observed upon deletion of the same C-terminal sequence of a single copy of aP0 (Figure 2D, bar 3). These results suggest that the C-terminal regions of multiple copies of aP1 make a major contribution to activation of ATP hydrolysis.

Structural basis for interaction of the aP1 stalk protein with aABCE1

Based on the binding data, we used an aP-C18 peptide consisting of 18 amino acid residues from the C-terminus of aP1 for co-crystallization with ADP-bound aABCE1. We failed to crystallize the complex with full-length aABCE1, presumably because of inhomogeneities resulting from in-

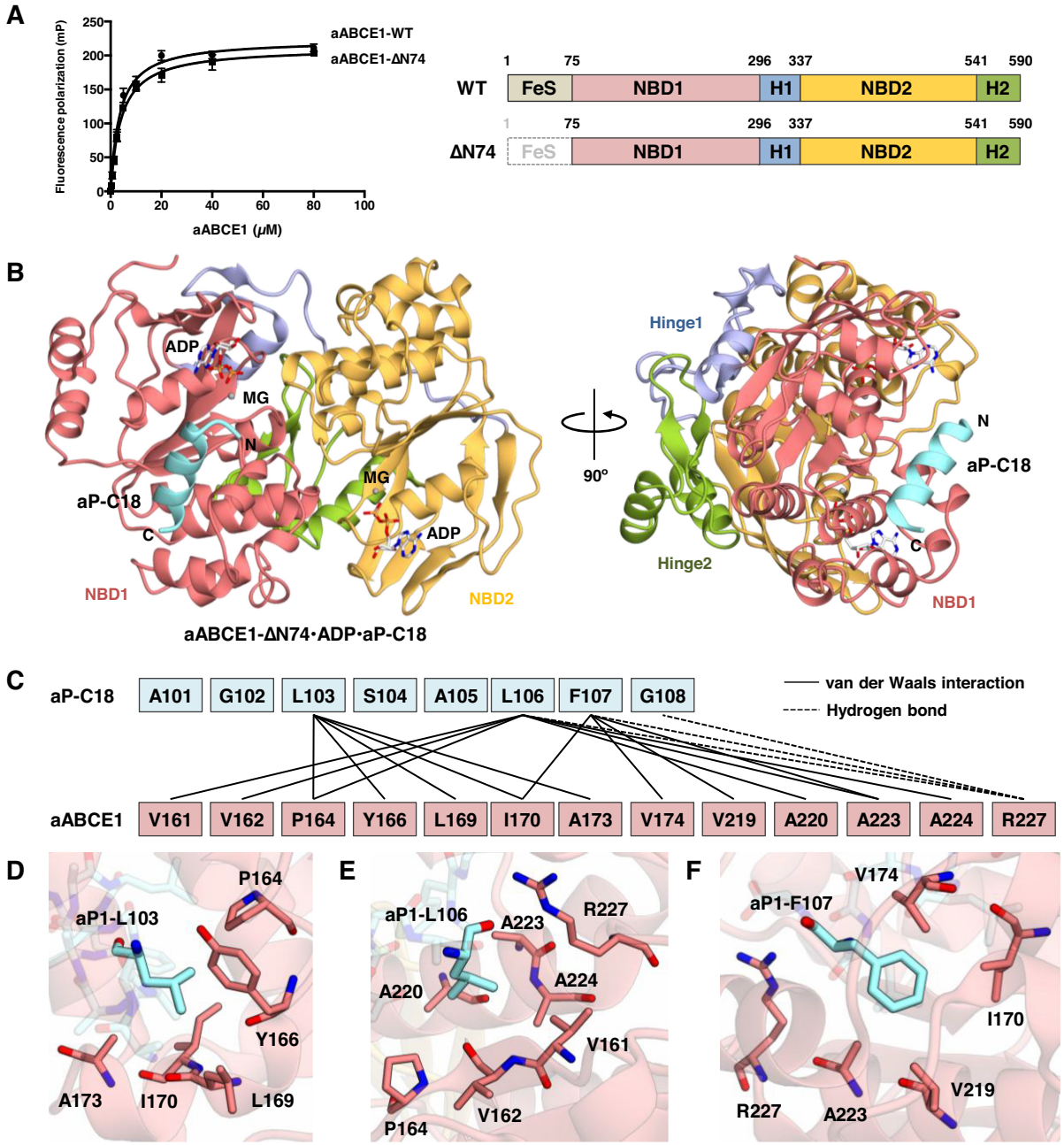

Figure 3. Crystal structure of the aABCE1-ΔN74•ADP•aP-C18 complex. (**A**) Left, Fluorescence polarization assay for binding of the FITC-labeled aP-C18 peptide to aABCE1 (WT and ΔN74-mutant). The labeled peptide was mixed with various concentrations of aABCE1 samples, and mP values were determined at each protein concentration. The averages and standard errors of three independent experiments are shown. Right, schematic representation of domain composition. (**B**) The overall structure of the aABCE1-ΔN74•ADP•aP-C18 complex at 2.1 Å resolution. The structures of aABCE1-ΔN74 and aP-C18 are represented by ribbon models. Colors are as follows: aABCE1 NBD1 (red), hinge1 (blue), NBD2 (yellow), hinge2 (light green), aP-C18 (light blue). (**C**) Schematic diagram of the interactions between aP-C18 and aABCE1. The van der Waals contacts and hydrogen bonds (<4 Å) are represented by solid lines and dashed lines, respectively. (**D**–**F**) Structure of the binding interface between aABCE1 and aP1-L103 (D), L106 (E) and F107 (F).

complete assembly or oxidation of the FeS clusters (13,14). We therefore constructed a aABCE1-ΔN74 truncation mutant lacking the FeS domain (residues 1–74), which binds equally as well to the aP-C18 peptide as does the full-length aABCE1 (Figure 3A and Table 1). As a result, crystals of aABCE1-ΔN74•ADP•aP-C18 ternary complex were obtained. The structure was determined by the molecular replacement method, and was refined at 2.1 Å resolution to an *R*-factor of 19.4% and a free *R*-factor of 24.4%. The data collection and structure refinement statistics are summarized in Supplementary Table S1.

In the aABCE1-ΔN74•ADP•aP-C18 complex, aP-C18 adopts an α-helical structure and binds to the surface cavity of NBD1 of aABCE1 (Figure 3B and Supplementary Figure S3). At the binding site, L103, L106 and F107 of aP1 interact with various amino acid residues of aABCE1, mainly

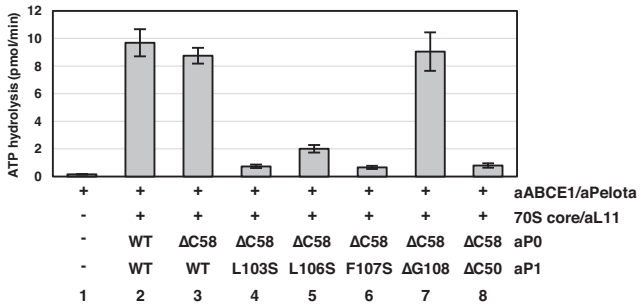

Figure 4. Crucial role of the C-terminal hydrophobic residues in aP1 in ATPase activation of aABCE1. The hybrid ribosomes were formed and the ribosome-dependent ATPase activity of aABCE1 was assayed in the same way as Figure 2D, except that the following aP1 mutants, together with aP0-ΔC58, were added: L103S (lane 4), L106S (lane 5), F107S (lane 6) and one in which the C-terminal G108 was removed (ΔG108). The averages and standard deviations of three independent experiments are shown. Bar 1, bar 2, bar 3 and bar 8 are the same data as presented by bar 1, bar 2, bar 3 and bar 5 of Figure 2D, respectively.

by hydrophobic interactions, i.e. L103 of aP1 interacts with P164, Y166, L169, I170 and A173 of aABCE1; L106 of aP1 interacts with V161, V162, P164, A220, A223, A224 and R227 of aABCE1; F107 of aP1 interacts with I170, V174, V219, A223 and R227 of aABCE1 (Figure 3C–F).

Effect of mutations on ATP hydrolysis and the binding of aABCE1 to aP1

The structure of the aABCE1-ΔN74•ADP•aP-C18 complex showed that L103, L106 and F107 of aP1 interact individually with several amino acid residues of aABCE1. To confirm these data, we first constructed the mutants aP1-L103S, L106S and F107S, and reconstituted the aP0•aP1 complex using the aP0-ΔC58 mutant, whose C-terminal 58 amino acid residues were deleted to eliminate the functional contribution of the C-terminal sequence of aP0 shared by aP1. The effect of aP1 mutations on aABCE1/ribosome-dependent ATPase activity was analyzed using the hybrid ribosome carrying the mutant aP0•aP1 complex (Figure 4). The marked effects of individual mutations indicate that hydrophobic amino acid residues at the C-terminal end region of aP1 are involved in binding to aABCE1 and its activation of ATP hydrolysis of aABCE1. In contrast, deletion of the amino acid G108 at the C-terminus of aP1 (ΔG108) produced no effect on ATPase activation. The largest effect on ATPase activity was observed with the mutation of F107 of aP1. We thus focused on interactions of F107 in aP1 with I170, V174, V219, A223 and R227 in aABCE1, and prepared the aABCE1 mutants I170S, V174S, V219S, A223S and R227A. The effects of the mutations were investigated by binding to aP-C18 peptide in a fluorescence polarization assay. As shown in Table 1 and Supplementary Figure S4, mutants I170S, V174S, A223S and R227A, but not V219S, resulted in impairment of binding to the aP1 peptide. These results are consistent with the crystal structural data.

aABCE1 is a twin ATPase comprised of NBD1 and NBD2, whose overall structures are similar to each other. However, we did not detect any electron density for aP-C18 within NBD2 in the crystal samples analyzed. By comparing the structures of NBD1 and NBD2, we found a difference between the two, namely, the aP1 binding site of NBD1 has an α-helix whereas the homologous region in NBD2 has a loop structure (Supplementary Figure S5A), that is the probable reason for the altered aP-C18 binding properties. To confirm further that NBD1 of aABCE1 is the main aP1 binding site, we introduced mutations at I408, Y412 and R470 in NBD2, which most likely correspond to the aP1 binding sites I170, V174 and R227 in NBD1 (Supplementary Figure S5B), and tested the effect on aP1 binding. The results showed that these mutations in NBD2 gave no marked effect on aP1 binding (Supplementary Figure S5C), suggesting that the preferential aP1 binding site is located in NBD1 within aABCE1.

Significance of interaction between ABCE1 and the stalk protein in viability of eukaryotic cells and ribosome splitting

A sequence alignment of archaeal/eukaryotic ABCE1 (Rli1 in yeast) showed that three hydrophobic amino acids of aABCE1 (I170, V174 and A223), which interact with F107 of aP1, were conserved as hydrophobic residues between archaea and eukaryotes (Supplementary Figure S6). To confirm the significance of the interaction between Rli1 and yeast ribosomal stalk protein in the viability of yeast cells, we constructed a single copy vector for expressing Rli1-3S mutant in which I176, I180 and M234 corresponding to I170, V174 and A223 of aABCE1 respectively were all substituted with serine (Figure 5A). This construct was introduced into a budding yeast *rli1*-degron strain, in which chromosomally-encoded *RLI1* was placed under control of a galactose-inducible promoter and tagged with N-terminal ubiquitin followed by an arginine residue (P_{GAL1}-*UBI-R-FLAG-RLI1*) (Supplementary Figure S7A), according to previous reports (40,41). Western blot analysis using α-FLAG antibody confirmed that the abundance of the UBI-R-FLAG-Rli1 was <1% of steady state levels after inhibition of transcription in glucose media (Supplementary Figure S7B). The viability of the *rli1*-degron strain carrying the vector for expression of Rli1-3S was markedly impaired, compared to the vector for expression of Rli1-WT (Figure 5B). These results suggest that the interaction between the ribosomal stalk protein and Rli1 is essential for viability of budding yeast.

We also investigated the effect of the 3S mutation *in vitro* using isolated eIF6, Dom34, Rli1-WT and Rli1-3S mutant. The yeast 80S ribosomes were prepared, as described previously (34) (Supplementary Figure S7C). Using these samples, we measured ATPase activity of Rli1. Although Rli1-WT, and Rli1-3S showed a low level of intrinsic ATPase activity, there appears to be no effect of the mutation (Figure 5C, bars 1 and 2). In contrast, the 3S mutation reduced the level of ribosome-dependent ATP hydrolysis of Rli1, suggesting that interaction between Rli1 and the stalk protein is required for efficient ATP hydrolysis of Rli1 on the yeast 80S ribosome (Figure 5C, bars 4 and 5). To investigate further the direct effect of the 3S mutation on ribosome splitting, we performed a subunit dissociation experiment using sucrose gradient sedimentation. Dissociation of the 80S ribosomes into individual subunits was observed to be Rli1-dose-dependent up to a level of about 40% (Supplementary

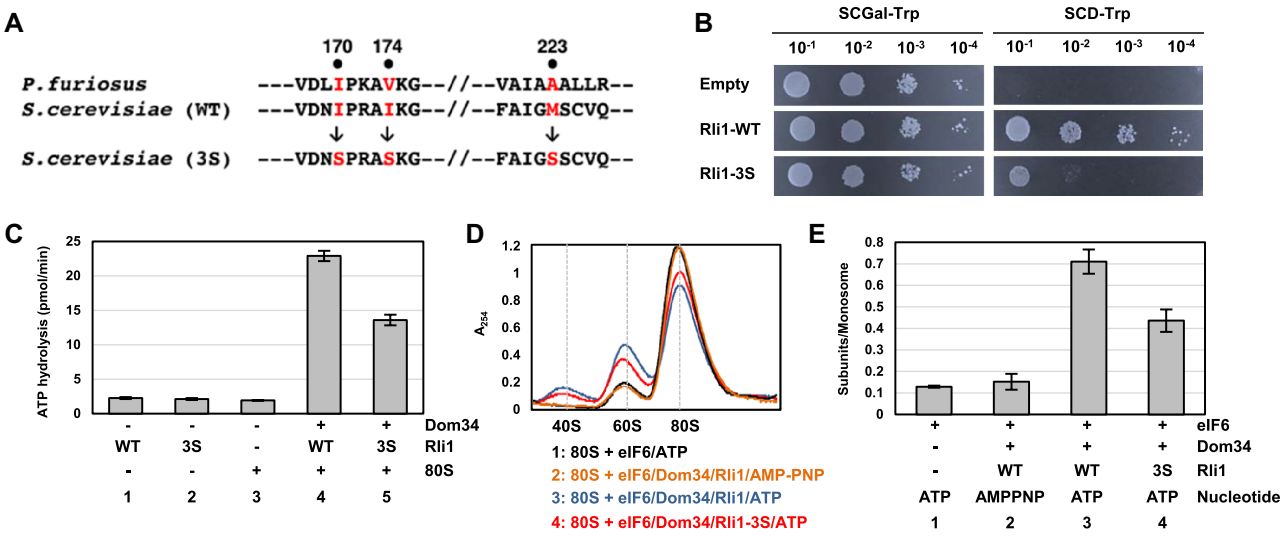

Figure 5. Effect of mutations at the conserved stalk binding site within yeast Rli1 on cell proliferation, ribosome-dependent ATP hydrolysis, and subunit dissociation. (**A**) Comparison of amino acids sequences of stalk binding site between *Pyrococcus furiosus* aABCE1 and *Saccharomyces cerevisiae* Rli1 (upper two sequences). Closed-circles indicate the amino acid residues of *P. furiosus* aABCE1 which interact with F107 of aP1. Sites of amino acid substitution in a Rli1 mutant (Rli1-3S) are shown (lower sequence). (**B**) Fixed amounts (5 μl of culture diluted to an OD_{600} of 0.5) of *rli1*-deg strain YTU2001 carrying the control vector (row 1) or the single copy plasmids expressing HA-tagged Rli1-WT (row 2) or Rli1-3S (row 3), and their 10-fold serial dilutions (OD_{600} = 0.05, 0.005 and 0.0005) were spotted onto SCGal-Trp (left) or SCD-Trp (right) medium for 3 or 2 days at 30°C, respectively. (**C**) ATP hydrolysis was measured in the presence of Rli1 alone (bar 1), Rli1-3S alone (bar 2), 80S alone (bar 3), Rli1/Dom34/80S (bar 4) and Rli1-3S/Dom34/80S (bar 5), as described in 'Materials and Methods' section. (**D**) 80S dissociation by Rli1, Dom34 and eIF6. 80S ribosomes were incubated with eIF6/ATP (peak 1: black), eIF6/Rli1/Dom34/AMP-PNP (peak 2: orange), eIF6/Rli1/Dom34/ATP (peak 3: blue) and eIF6/Rli1-3S/Dom34/ATP (peak 4: red). Each sample was analyzed by sucrose density gradient centrifugation. eIF6 was added to prevent reassembly. (**E**) The ratio between the two subunits and monosome was determined from the sedimentation profiles in (D), as described in 'Materials and Methods' section. The averages and standard deviations of three independent experiments are shown in (C) and (E).

Figure S7D and E). The efficiency of the dissociation was low in the 80S ribosome sample, presumably because of the presence of translating ribosomes as well as vacant 80S ribosomes. Despite the low dissociation rate, the results clearly show that the presence of eIF6, Dom34 and ATP, but not AMP-PNP, are required for the subunit dissociation (Figure 5D and E). These results are consistent with previous studies (7,8,10). Importantly, the 3S mutation reduced the level of subunit dissociation, and the degree of mutational effect on subunit dissociation was comparable to that on the ATPase activity (Figure 5C and E). These results suggest a significant role for the interaction between Rli1 and the stalk protein in ATPase activation and efficient ribosome splitting.

DISCUSSION

The ribosomal stalk proteins are classified into two divergent groups from the viewpoint of evolution—archaeal/eukaryotic and bacterial groups (42). The archaeal aP1 and eukaryotic P1/P2 are structurally related to each other. They have an unstructured C-terminal half (23) and contain a conserved L/GXXLF sequence motif located at the C-terminus, in contrast with the C-terminal region of bacterial L12 that adopts a stable globular structure (43,44). Recent studies revealed that the conserved L/GXXLF region of the stalk protein is the major binding site for archaeal (and presumably also eukaryotic) EF1A and EF2 (24,25). The present structural and biochemical analyses demonstrate that the C-terminal L/GXXLF region of the stalk protein directly binds to ABCE1 and participates in ATP hydrolysis activation. Because ABCE1 exists in archaea and eukaryotes and plays a crucial role in translation recycling, the present evidence suggests that the archaeal/eukaryotic stalk protein participates in the recycling mechanism in the archaeal/eukaryotic mode.

For crystallization in the present study, we used aABCE1-ΔN74 lacking the FeS domain and the C-terminal peptide of aP1, with the resulting structure of the complex identifying many amino acid residues of aABCE1 and aP1 involved in direct binding (Figure 3). Therefore, a role for the N-terminal FeS domain in binding to the stalk protein is not clear from the present crystal data. To verify the crystal structural data, we carefully examined the effect of mutations at putative aABCE1•aP1 binding sites based on the crystal data by assaying aABCE1•aP1 binding and ATPase activity using full-length aABCE1 and aP1 samples. Most of the biochemical data support the crystal structure data. Furthermore, aABCE1-ΔN74 has almost the same ability as intact aABCE1 in binding the C-terminal peptide of aP1. From these results, it is likely that our structural data based on crystallography of the truncated aABCE1 and aP1 reflect the actual aABCE1•aP1 interaction. We infer that the main functional role of the N-terminal FeS domain of aABCE1 is binding to aPelota (9) with subsequent ribosome splitting (18), while its direct contribution to aP1 binding seems to be low.

It is noteworthy that the same C-terminal hydrophobic region of aP1 binds to the recycling factor aABCE1 as well as to the elongation factors aEF1A and aEF2,

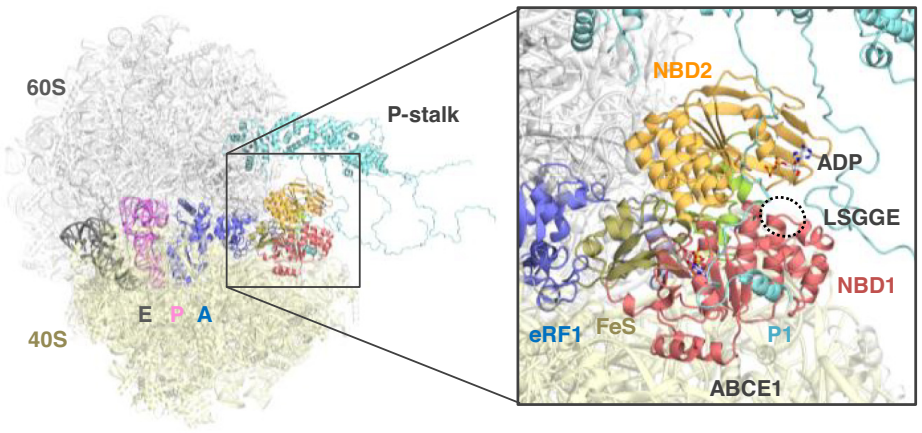

Figure 6. The model of aABCE1•aP-C18 complex docking with the 80S pre-splitting complex. Colors are as follows: 60S (white), 40S (light yellow), stalk complex (light blue), eRF1 (dark blue), peptidyl-tRNA (magenda), deacyl-tRNA (dark green), aABCE1-FeS (khaki), aABCE1-NBD1 (red), aABCE1-Hinge1 (blue), aABCE1-NBD2 (yellow), aABCE1-Hinge2 (light green). In the docking model, we first made the full-length aABCE1•aP-C18 complex using the complete X-ray structure of aABCE1 from *Pyrococcus abyssi* [PDB code: 3BK7] (14) and superimposed it onto the eukaryotic 80S pre-splitting complex with eABCE1 and eRF1 [PDB code: 5LZV] (17). Subsequently the aP0•aP1 stalk complex core from *Pyrococcus horikoshii* [PDB code: 3A1Y] (21) was superimposed onto the model. The aP0•aP1 stalk complex core and aP-C18 bound to aABCE1 were connected by the flexible hinge region of aP1. Other hinge regions of aP0 and aP1 were modeled arbitrarily. In this docking model, aABCE1 represents an open-state. The dashed-circled region is the LSGGE motif of NBD1.

and participates in activation of ATP hydrolysis as well as GTP hydrolysis. Comparison of the present structural data of aP1•aABCE1 with previous structural data for aP1•aEF1A (25) shows that there is no conformational similarity between aP1 binding sites in the two factors (Supplementary Figure S8). A noticeable resemblance between the two aP1 binding pockets is hydrophobicity, which seems to stabilize the α-helix structure of the C-terminal region of aP1. However, the length of the α-helix of the C-terminal regions formed is different between the two complexes. Given the unstructured properties of the C-terminal region of the archaeal/eukaryotic stalk protein, we infer that a different length of helix-like structure can be induced upon binding to different factors. This induced-fit docking mechanism may be able to explain the ability of the stalk protein to bind to multiple factors.

It is believed that the extended C-terminal half of the stalk protein is flexible and moves around the ribosome, and once the C-terminal L/GXXLF region binds to a translational GTPase, the stalk protein seems to guide the factor to the factor binding center of the ribosome giving proper orientation of the factor. Our present results suggest that the stalk protein also recruits aABCE1 to the factor binding center using the same recruitment mechanism as GTPase factors. To confirm this hypothesis from a structural view point, we constructed a docking model, using the structures of the eukaryotic pre-splitting ribosome associated with eABCE1 and eRF1 (17) and the archaeal stalk protein complex (21) (Figure 6). In this model, the aP1-binding site within NBD1 of aABCE1 is facing outward. Thus, the C-terminal region of aP1 can reach the ribosome-associated aABCE1 via the flexible C-terminal half of aP1 without steric hindrance. The present docking model therefore supports the role of the stalk protein in leading the factor to the site around the ribosomal factor binding center and giving proper orientation.

It is known that the SRL of 23S/28S rRNA participates in GTP hydrolysis by translational GTPase factors (45–47). Our footprinting studies with hybrid ribosome systems have also confirmed that A2660 and A2665 in the SRL of 23S rRNA are protected by archaeal and eukaryotic elongation factors dependent on the presence of archaeal and eukaryotic stalk proteins, respectively (26,27). However, aABCE1 gives no footprint in the SRL region (Supplementary Figure S9) in the hybrid ribosome carrying the archaeal stalk in the present study, although the hybrid ribosome has the ability to bind aABCE1 (Supplementary Figure S2) and activate ATP hydrolysis (Figure 1B). This result is consistent with previous cryo-EM data showing no contact of aABCE1 with the SRL in the ribosome•ABCE1 complex (15). It is therefore likely that ATPase activation of aABCE1 occurs via an unknown mechanism different form that of GTPase factors involving the SRL.

Because our crystal structural data shows the aP1 binding site is rather far away from both the ATP binding sites in NBD1 (NBS I) and NBD2 (NBS II), it also seems unlikely that the C-terminal end region directly participates in ATPase activation. Previous work by Barthelme *et al.* (9) may provide a hint about the ATPase activation mechanism. They analyzed intrinsic ATP hydrolysis of aABCE1 isolated from *Sulfolobus solfataricus* and its mutants, and showed that ATP binding sites in NBD1 and NBD2 are structurally and functionally asymmetric, and that ATPase activity of NBS I is strongly stimulated by a mutation, E485Q, in the Walker B motif in NBD2, that results in ATP occlusion in NBS II (9). Considering this point of view and our crystal structural model of the aP1•aABCE1 complex, in which aP1 binds to the cleft behind the conserved LSGGE motif region in NBD1 (Figure 3B), we propose the following working hypothesis for ATPase activation. Since the LSGGE regions are involved in the recognition of γ-phosphate of ATP and inducing the NBD1/NBD2 closing

state (48–50), we infer that the aP1 binding to aABCE1 on the ribosome may affect a structural feature of the LSGGE region in NBD1 and stabilize the ATP binding to NBS II. Thus, the aP1 binding may participate in the ATP occlusion in NBS II of aABCE1 that activates ATP hydrolysis at NBS I. Further extensive studies including structural analysis for both ATP- and ADP-bound forms of full-length aABCE1 are needed for deeper insight into the exact role of the ribosomal stalk protein in ATPase activation and in ribosome recycling.

DATA AVAILABILITY

The structural coordinates of the refined model and the structure factors have been deposited in the RCSB Protein Data Bank (www.rcsb.org/) and assigned the identifier 5YV5.

SUPPLEMENTARY DATA

Supplementary Data are available at NAR Online.

ACKNOWLEDGEMENTS

We thank AP Schuller and R Green (Johns Hopkins University School of Medicine) for providing the Rli1 expression plasmid and protocol for its purification. We thank H Moriya (Okayama University) for providing the pTOW-pGFP plasmid. We thank T Endo (Kyoto Sangyo University) for providing the anti-Tom40 antibody.

FUNDING

Grant-in-Aid for JSPS Fellows [16J01001 to H.I.]; Grant-in-Aid for Scientific Research (B) [16H04741 to T.U.]; Grant-in-Aid for Scientific Research (C) [15K06964 to K.I.]; Japan Society for the Promotion of Science. Funding for open access charge: Ministry of Education, Culture, Sports, Science and Technology; Japan Society for the Promotion of Science.
Conflict of interest statement. None declared.

REFERENCES

1. Kapp,L.D. and Lorsch,J.R. (2004) The molecular mechanics of eukaryotic translation. *Annu. Rev. Biochem.*, **73**, 657–704.
2. Rodnina,M.V. and Wintermeyer,W. (2009) Recent mechanistic insights into eukaryotic ribosomes. *Curr. Opin. Cell Biol.*, **21**, 435–443.
3. Liljas,A. and Ehrenberg,M. (2013) The catalysts—-translation factors. In: *Structural Aspects of Protein Synthesis*. 2nd edn. World Scientific, Singapore, pp. 149–228.
4. Mohr,D., Wintermeyer,W. and Rodnina,M.V. (2002) GTPase activation of elongation factors Tu and G on the ribosome. *Biochemistry*, **41**, 12520–12528.
5. Diaconu,M., Kothe,U., Schlünzen,F., Fischer,N., Harms,J.M., Tonevitsky,A.G., Stark,H., Rodnina,M.V. and Wahl,M.C. (2005) Structural basis for the function of the ribosomal L7/12 stalk in factor binding and GTPase activation. *Cell*, **121**, 991–1004.
6. Nürenberg,E. and Tampé,R. (2013) Tying up loose ends: ribosome recycling in eukaryotes and archaea. *Trends Biochem. Sci.*, **38**, 64–74.
7. Pisarev,A.V., Skabkin,M.A., Pisareva,V.P., Skabkina,O.V., Rakotondrafara,A.M., Hentze,M.W., Hellen,C.U. and Pestova,T.V. (2010) The role of ABCE1 in eukaryotic posttermination ribosomal recycling. *Mol. Cell*, **37**, 196–210.
8. Shoemaker,C.J. and Green,R. (2011) Kinetic analysis reveals the ordered coupling of translation termination and ribosome recycling in yeast. *Proc. Natl. Acad. Sci. U.S.A.*, **108**, E1392–E1398.
9. Barthelme,D., Dinkelaker,S., Albers,S.V., Londei,P., Ermler,U. and Tampé,R. (2011) Ribosome recycling depends on a mechanistic link between the FeS cluster domain and a conformational switch of the twin-ATPase ABCE1. *Proc. Natl. Acad. Sci. U.S.A.*, **108**, 3228–3233.
10. Pisareva,V.P., Skabkin,M.A., Hellen,C.U., Pestova,T.V. and Pisarev,A.V. (2011) Dissociation by Pelota, Hbs1 and ABCE1 of mammalian vacant 80S ribosomes and stalled elongation complexes. *EMBO J.*, **30**, 1804–1817.
11. van den Elzen,A.M., Schuller,A., Green,R. and Séraphin,B. (2014) Dom34-Hbs1 mediated dissociation of inactive 80S ribosomes promotes restart of translation after stress. *EMBO J.*, **33**, 265–276.
12. Strunk,B.S., Novak,M.N., Young,C.L. and Karbstein,K. (2012) A translation-like cycle is a quality control checkpoint for maturing 40S ribosome subunits. *Cell*, **150**, 111–121.
13. Karcher,A., Büttner,K., Märtens,B., Jansen,R.P. and Hopfner,K.P. (2005) X-ray structure of RLI, an essential twin cassette ABC ATPase involved in ribosome biogenesis and HIV capsid assembly. *Structure*, **13**, 649–659.
14. Karcher,A., Schele,A. and Hopfner,K.P. (2008) X-ray structure of the complete ABC enzyme ABCE1 from *Pyrococcus abyssi*. *J. Biol. Chem.*, **283**, 7962–7971.
15. Becker,T., Franckenberg,S., Wickles,S., Shoemaker,C.J., Anger,A.M., Armache,J.P., Sieber,H., Ungewickell,C., Berninghausen,O., Daberkow,I. *et al.* (2012) Structural basis of highly conserved ribosome recycling in eukaryotes and archaea. *Nature*, **482**, 501–506.
16. Preis,A., Heuer,A., Barrio-Garcia,C., Hauser,A., Eyler,D.E., Berninghausen,O., Green,R., Becker,T. and Beckmann,R. (2014) Cryoelectron microscopic structures of eukaryotic translation termination complexes containing eRF1-eRF3 or eRF1-ABCE1. *Cell Rep.*, **8**, 59–65.
17. Brown,A., Shao,S., Murray,J., Hegde,R.S. and Ramakrishnan,V. (2015) Structural basis for stop codon recognition in eukaryotes. *Nature*, **524**, 493–496.
18. Heuer,A., Gerovac,M., Schmidt,C., Trowitzsch,S., Preis,A., Kötter,P., Berninghausen,O., Becker,T., Beckmann,R. and Tampé,R. (2017) Structure of the 40S-ABCE1 post-splitting complex in ribosome recycling and translation initiation. *Nat. Struct. Mol. Biol.*, **24**, 453–460.
19. Franckenberg,S., Becker,T. and Beckmann,R. (2012) Structural view on recycling of archaeal and eukaryotic ribosomes after canonical termination and ribosome rescue. *Curr. Opin. Struct. Biol.*, **22**, 786–789.
20. Maki,Y., Hashimoto,T., Zhou,M., Naganuma,T., Ohta,J., Nomura,T., Robinson,C.V. and Uchiumi,T. (2007) Three binding sites for stalk protein dimers are generally present in ribosomes from archaeal organism. *J. Biol. Chem.*, **282**, 32827–32833.
21. Naganuma,T., Nomura,N., Yao,M., Mochizuki,M., Uchiumi,T. and Tanaka,I. (2010) Structural basis for translation factor recruitment to the eukaryotic/archaeal ribosomes. *J. Biol. Chem.*, **285**, 4747–4756.
22. Hagiya,A., Naganuma,T., Maki,Y., Ohta,J., Tohkairin,Y., Shimizu,T., Nomura,T., Hachimori,A. and Uchiumi,T. (2005) A mode of assembly of P0, P1, and P2 proteins at the GTPase-associated center in animal ribosome: *in vitro* analysis with P0 truncation mutants. *J. Biol. Chem.*, **280**, 39193–39199.
23. Lee,K.M., Yusa,K., Chu,L.O., Yu,C.W., Oono,M., Miyoshi,T., Ito,K., Shaw,P.C., Wong,K.B. and Uchiumi,T. (2013) Solution structure of human P1•P2 heterodimer provides insights into the role of eukaryotic stalk in recruiting the ribosome-inactivating protein trichosanthin to the ribosome. *Nucleic Acids Res.*, **41**, 8776–8787.
24. Nomura,N., Honda,T., Baba,K., Naganuma,T., Tanzawa,T., Arisaka,F., Noda,M., Uchiyama,S., Tanaka,I., Yao,M. *et al.* (2012) Archaeal ribosomal stalk protein interacts with translation factors in a nucleotide-independent manner via its conserved C terminus. *Proc. Natl. Acad. Sci. U.S.A.*, **109**, 3748–3753.
25. Ito,K., Honda,T., Suzuki,T., Miyoshi,T., Murakami,R., Yao,M. and Uchiumi,T. (2014) Molecular insights into the interaction of the ribosomal stalk protein with elongation factor 1α. *Nucleic Acids Res.*, **42**, 14042–14052.
26. Uchiumi,T., Honma,S., Endo,Y. and Hachimori,A. (2002) Ribosomal proteins at the stalk region modulate functional rRNA structures in the GTPase center. *J. Biol. Chem.*, **277**, 41401–41409.

27. Imai,H., Miyoshi,T., Murakami,R., Ito,K., Ishino,Y. and Uchiumi,T. (2015) Functional role of the C-terminal tail of the archaeal ribosomal stalk in recruitment of two elongation factors to the sarcin/ricin loop of 23S rRNA. *Genes Cells*, **20**, 613–624.
28. Nomura,T., Nakano,K., Maki,Y., Naganuma,T., Nakashima,T., Tanaka,I., Kimura,M., Hachimori,A. and Uchiumi,T. (2006) *In vitro* reconstitution of the GTPase-associated centre of the archaebacterial ribosome: the functional features observed in a hybrid form with *Escherichia coli* 50S subunits. *Biochem. J.*, **396**, 565–571.
29. Frolova,L., Le Goff,X., Zhouravleva,G., Davydova,E., Philippe,M. and Kisselev,L. (1996) Eukaryotic polypeptide chain release factor eRF3 is an eRF1- and ribosome-dependent guanosine triphosphatase. *RNA*, **2**, 334–341.
30. Kabsch,W. (2010) XDS. *Acta Crystallogr. D Biol. Crystallogr.*, **66**, 125–132.
31. Long,F., Vagin,A.A., Young,P. and Murshudov,G.N. (2008) BALBES: a molecular-replacement pipeline. *Acta Crystallogr. D Biol. Crystallogr.*, **64**, 125–132.
32. Emsley,P. and Cowtan,K. (2004) Coot: model-building tools for molecular graphics. *Acta Crystallogr. D Biol. Crystallogr.*, **60**, 2126–2132.
33. Murshudov,G.N., Skubák,P., Lebedev,A.A., Pannu,N.S., Steiner,R.A., Nicholls,R.A., Winn,M.D., Long,F. and Vagin,A.A. (2011) REFMAC5 for the refinement of macromolecular crystal structures. *Acta Crystallogr. D Biol. Crystallogr.*, **67**, 355–367.
34. Shin,B.S. and Dever,T.E. (2007) Molecular genetic structure-function analysis of translation initiation factor eIF5B. *Methods Enzymol.*, **429**, 185–201.
35. Peltz,S.W., Donahue,J.L. and Jacobson,A. (1992) A mutation in the tRNA nucleotidyltransferase gene promotes stabilization of mRNAs in *Saccharomyces cerevisiae*. *Mol. Cell. Biol.*, **12**, 5778–5784.
36. Miyoshi,T. and Uchiumi,T. (2008) Functional interaction between bases C1049 in domain II and G2751 in domain VI of 23S rRNA in *Escherichia coli* ribosomes. *Nucleic Acids Res.*, **36**, 1783–1791.
37. Motohashi,K. (2015) A simple and efficient seamless DNA cloning method using SLiCE from *Escherichia coli* laboratory strains and its application to SLiP site-directed mutagenesis. *BMC Biotechnol.*, **15**, 47.
38. Ballesta,J.P., Rodriguez-Gabriel,M.A., Bou,G., Briones,E., Zambrano,R. and Remacha,M. (1999) Phosphorylation of the yeast ribosomal stalk. Functional effects and enzymes involved in the process. *FEMS Microbiol. Rev.*, **23**, 537–550.
39. Uchiumi,T., Honma,S., Nomura,T., Dabbs,E.R. and Hachimori,A. (2002) Translation elongation by a hybrid ribosome in which proteins at the GTPase center of the *Escherichia coli* ribosome are replaced with rat counterparts. *J. Biol. Chem.*, **277**, 3857–3862.
40. Young,D.J., Guydosh,N.R., Zhang,F., Hinnebusch,A.G. and Green,R. (2015) Rli1/ABCE1 recycles terminating ribosomes and controls translation reinitiation in 3′UTRs in vivo. *Cell*, **162**, 872–884.
41. Serdar,L.D., Whiteside,D.L. and Baker,K.E. (2016) ATP hydrolysis by UPF1 is required for efficient translation termination at premature stop codons. *Nat. Commun.*, **7**, 14021.
42. Grela,P., Bernadó,P., Svergun,D., Kwiatowski,J., Abramczyk,D., Grankowski,N. and Tchórzewski,M. (2008) Structural relationships among the ribosomal stalk proteins from the three domains of life. *J. Mol. Evol.*, **67**, 154–167.
43. Leijonmarck,M. and Liljas,A. (1987) Structure of the C-terminal domain of the ribosomal protein L7/L12 from *Escherichia coli* at 1.7 A. *J. Mol. Biol.*, **195**, 555–579.
44. Bocharov,E.V., Sobol,A.G., Pavlov,K.V., Korzhnev,D.M., Jaravine,V.A., Gudkov,A.T. and Arseniev,A.S. (2004) From structure and dynamics of protein L7/L12 to molecular switching in ribosome. *J. Biol. Chem.*, **279**, 17697–17706.
45. Moazed,D., Robertson,J.M. and Noller,H.F. (1988) Interaction of elongation factors EF-G and EF-Tu with a conserved loop in 23S RNA. *Nature*, **334**, 362–364.
46. Clementi,N., Chirkova,A., Puffer,B., Micura,R. and Polacek,N. (2010) Atomic mutagenesis reveals A2660 of 23S ribosomal RNA as key to EF-G GTPase activation. *Nat. Chem. Biol.*, **6**, 344–351.
47. Voorhees,R.M., Schmeing,T.M., Kelley,A.C. and Ramakrishnan,V. (2010) The mechanism for activation of GTP hydrolysis on the ribosome. *Science*, **330**, 835–838.
48. Chen,J., Lu,G., Lin,J., Davidson,A.L. and Quiocho,F.A. (2003) A tweezers-like motion of the ATP-binding cassette dimer in an ABC transport cycle. *Mol. Cell*, **12**, 651–661.
49. Hanekop,N., Zaitseva,J., Jenewein,S., Holland,I.B. and Schmitt,L. (2006) Molecular insights into the mechanism of ATP-hydrolysis by the NBD of the ABC-transporter HlyB. *FEBS Lett.*, **580**, 1036–1041.
50. Hopfner,K.P. (2016) Invited review: Architectures and mechanisms of ATP binding cassette proteins. *Biopolymers*, **105**, 492–504.